ACS OMEGA

http://pubs.acs.org/journal/acsodf

Article

Millimeter-Scale Continuous Film of MoS_2 Synthesized Using a Mo, Na, and Seeding Promoter-Based Coating as a Solid Precursor

Maddumage Don Sandeepa Lakshad Wimalananda, Jae-Kwan Kim, Sung Woon Cho,* and Ji-Myon Lee*

Cite This: *ACS Omega* 2021, 6, 32208−32214

Read Online

ACCESS | Metrics & More | Article Recommendations | Supporting Information

ABSTRACT: While the chemical vapor deposition technique can be used to fabricate 2D materials in a larger area, materials like MoS_2 have limited controllability due to their lack of self-controlling nature. This article presents a new technique for synthesizing a void-free millimeter-scale continuous monolayer MoS_2 film through the diffusion of a well-controlled Mo, Na, and seeding promoter-based coating under a low-pressure N_2 atmosphere. Compared to the conventional method, this technique provides precise control of solid precursors, where MoS_2 grows next to the coating. At 800 °C, the synthesized MoS_2 showed a uniform single-layer MoS_2 film; however, a Na-free coating showed nanoscale voids and poor crystal quality, which are attributed to a higher edge-attachment barrier that slows down the MoS_2 lateral growth. The synthesized MoS_2 with Na-containing solution showed an intense PL peak with a 1.86 eV band gap. Even at the relatively low temperature of 700 °C, compared to the Na-excluded condition, MoS_2 showed almost two times higher area coverage with a comparatively larger crystal size. This finding may assist in the future development of MoS_2-based electronic and optoelectronic devices such as transistors and photodetectors.

INTRODUCTION

The invention of graphene synthesis has driven nano−micro devices to an atomically thin scale. Graphene is a semimetal with a zero band gap at the direct point; thus, bilayer graphene shows band gap tenability up to a certain level.[1,2] Recently, transition metal dichalcogenides (TMDs) like MoS_2 and WSe_2 have shown excellent semiconductor characteristics as an atomically thin-layered material.[3−5] Therefore, TMDs as ultrathin materials have shown a significant potential for use in modern layered devices like transistors, photodetectors, and light-emitting devices.

Like graphene, TMDs can also be synthesized using the chemical vapor deposition (CVD) technique with similar merits, notably a broader growth area and larger 2D crystal size.[6−9] However, compared to graphene synthesis, TMDs show a deficiency of self-limiting behavior along with difficulty in 2D crystal formation.[10−13] In general, the nucleation of TMDs on surfaces like SiO_2/Si requires proper wettability.[10] Nevertheless, the seeding agents and improved surface wettability (for TMDs) on such surfaces showed a nucleation tendency.[10]

Previous studies suggest that seeding promoters like PTAS (perylene 3,4,9,10-tetracarboxylic potassium salt) work well on hydrophilic surfaces and that F_{16}CuPc (copper(II) 1,2,3,4,8,9,10,11,15,16,17,18,22,23,24,25-hexadecafluoro-29*H*,31*H*-phthalocyanine) works well even on hydrophobic surfaces.[14] Seeding promoters increase the surface adhesive force of TMDs, which results in the formation of heterogeneous nucleation sites for TMDs and 2D crystal formation.[14] According to Ling et al., the use of seeding promoters lowers the nucleation barrier of TMDs on the surface.[14] Therefore, with the presence of a seeding promoter, TMDs can be synthesized at lower temperatures.[14]

Ideally, larger TMD crystals can be synthesized by a lower number of nuclei with rapid growth under any mass flux rate.[10] Further, a rapid growth rate eases larger crystal formation and reduces the multilayer TMD traces.[10] There is currently substantial interest in supporting metallic ions such as Na^+ in MoS_2 synthesis because Na^+ lowers the edge-attachment barrier of MoS_2 for rapid synthesis; the effect of Na^+ has previously been studied for liquid substrates and the vapor−liquid−solid phase synthesis method.[13,15]

Received: September 13, 2021
Accepted: November 8, 2021
Published: November 16, 2021

The primary issue of TMD synthesis dealt with in this paper is the dependability of mass flux on the TMD properties. Therefore, even under conditions of controlled nucleation and rapid growth, the mass flow should be well controlled in terms of the amount and distance to the solid precursor.[10] Liquid-phase substrates like glass substrates, where metal ions are first dissolved in molten glass and then diffuse to the substrate surface for 2D crystal growth, are an attractive solution to this issue.[13,15] This leads to better controllability; however, it requires a transfer process that may damage the crystal quality.

The article focuses on the direct synthesis of MoS_2 on SiO_2/Si by limiting metal ions to a selected area. A novel concept is introduced, which involves fabricating a millimeter-scale continuous and monolayer MoS_2 film using a NaCl-, $F_{16}CuPC$-, and MoO_3-based solid coating. The special use of Na^+ for void-free MoS_2 film synthesis is discussed as well. The concept can be used to synthesize the millimeter-scale MoS_2 film for 2D van der Waals heterostructures for transistor and photodetector applications.

RESULTS AND DISCUSSION

Synthesis of Millimeter-Scale Continuous Film of MoS_2. The use of seeding promoters is necessary for the fabrication of MoS_2 2D films on SiO_2/Si. In general, $F_{16}CuPc$ is deposited by a thermal evaporation process,[14] while this work uses a low concentration of $F_{16}CuPc$ in liquid solution. To bring every necessary ingredient into liquid form, both MoO_3 and NaCl are dissolved in NH_4OH. MoO_3 dissolves in NH_4OH by forming $(NH_4)_2MoO_4$,[13] and NaCl makes an equilibrium with NH_4OH. Although NH_4OH is not a good solvent for $F_{16}CuPc$, a shallow concentration of $F_{16}CuPc$ (1 mg in 100 mL of NH_4OH) shows reasonable solubility, making a light greenish solution (Figure S1a–c of the Supporting Information (SI)). The 2 μL of the solution approximately includes 40 nmol of Mo ions, 200 nmol of Na ions, and 20 pmol of $F_{16}CuPc$. Figure S2a of the SI shows the FE-SEM image of the material-coated area following deposition on the substrate. Figure S2b of the SI shows an EDX diagram, which confirms the existence of all Mo, Na, and Cu (from $F_{16}CuPc$) ions.

To elucidate the effects of $F_{16}CuPc$ and Na ion, MoS_2 was synthesized at 800 °C for 3 min. MoS_2 was grown through the diffusion of limited $F_{16}CuPc$, Mo, and Na; Figure 1 shows a schematic diagram. Figure 2a–c represents the synthesized MoS_2 with different solutions: one solution was prepared with all ingredients (Figure 2c), while another two solutions were prepared by excluding $F_{16}CuPc$ (Figure 2a) and Na (Figure 2b). The same Mo concentration was maintained in all of the solutions.

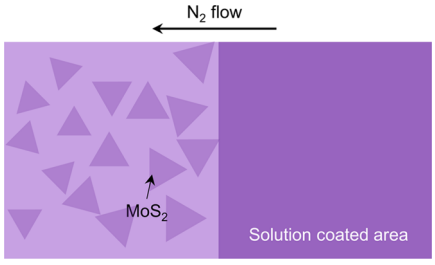

Figure 1. Schematic diagram of the diffusion-driven MoS_2 growth (image not to scale).

The $F_{16}CuPc$-excluded sample only showed MoS_2 nanoparticles. Though MoS_2 nuclei were formed on the piranha-treated surface, the 2D crystal growth was diminished. Both the Na-included and -excluded samples showed a continuous film of MoS_2 according to optical microscopy. Several OM images (Figure S3) were taken in different positions from the coating (the sample indicating all of Na, Mo, and seeding promoters), such as near the coating (Figure S3a,b) as well as at distances of 0.5 mm (Figure 2c), 2 mm (Figure S3c), and 3 mm (Figure S3d). All of the OM images confirmed the continuous nature of MoS_2. Therefore, the synthesized MoS_2 can be considered to be a continuous film that is suitable for millimeter-scale regions.

The AFM inset of Figure 2b shows the discreet behavior (voids) of the Na-excluded sample compared to that of the Na-included sample (Figure 2c). A possible reason for the formation of a void-free continuous film of MoS_2 is that the reduced edge-attachment barrier increased the possibility of expanding the MoS_2 film. Further, compared to the conventional film, during the alkali ion-assisted growth, Mo and S ions can easily be attached to defected areas (edges), thereby fabricating void-free MoS_2 film growth.

In addition, the film thickness was 0.6–0.7 nm. Figure 2d–f shows the Raman spectra of the fabricated MoS_2 on SiO_2/Si. The gap between A_{1g} and E^1_{2g} Raman excitement represents the number of MoS_2 layers; in general, the monolayer MoS_2 reported 19–20 cm^{-1}, while the multilayer MoS_2 reported 24–26 cm^{-1} of A_{1g}–E^1_{2g}.[3,16−18] Therefore, the AFM and Raman characteristics indicate that the $F_{16}CuPc$-included samples show a 2D crystal growth tendency, while the $F_{16}CuPc$-excluded sample shows the shape of the MoS_2 nanoparticle, which has multilayer Raman characteristics.

Both MoS_2 films presented in Figure 2b,c showed surface roughness R_q (root mean square) below 0.1 nm, where the substrate showed R_q of approximately 0.2 nm. However, observing the voids of the Na-excluded sample (compared to the Na-included sample) confirms the effect of Na in achieving better continuity of the MoS_2 film through a diffusion-based approach. Further, the purity of the representative sample in Figure 2c was tested. Figure S2f shows an EDX diagram of the synthesized MoS_2 (approximately 0.5 mm away from the coating). According to the EDX analysis, less than 0.1% of Na and Cu atoms exist, thus confirming the better purity of the synthesized MoS_2.

The effect of alkali ions on the crystal quality of the synthesized MoS_2 was characterized using Raman LA excitation. Figure 3a shows the Raman spectra of the Na ion-included and -excluded sample. According to a previous article, the LA peak intensity is influenced by the interdefect distance[19] and the $\frac{I_{LA}}{I_{A_{1g}}}$ ratio decreases with the improved MoS_2 crystal quality. According to Figure 3a, the Na-included sample shows a much lower $\frac{I_{LA}}{I_{A_{1g}}}$ ratio, and the LA peak is hardly visible compared to that in the alkali ion-free sample, indicating that the effect on the alkali ion improved the crystal quality of MoS_2. The stability of MoS_2 was also tested. Finally, the sample was exposed to an ambient atmosphere for 30 days, and the Raman characteristics were rechecked. Figure 3a shows the representative Raman spectra, which show no significant change in Raman characteristics (the values of $\left(\frac{I_{LA}}{I_{A_{1g}}}\right)$ are

https://doi.org/10.1021/acsomega.1c05052
ACS Omega 2021, 6, 32208−32214

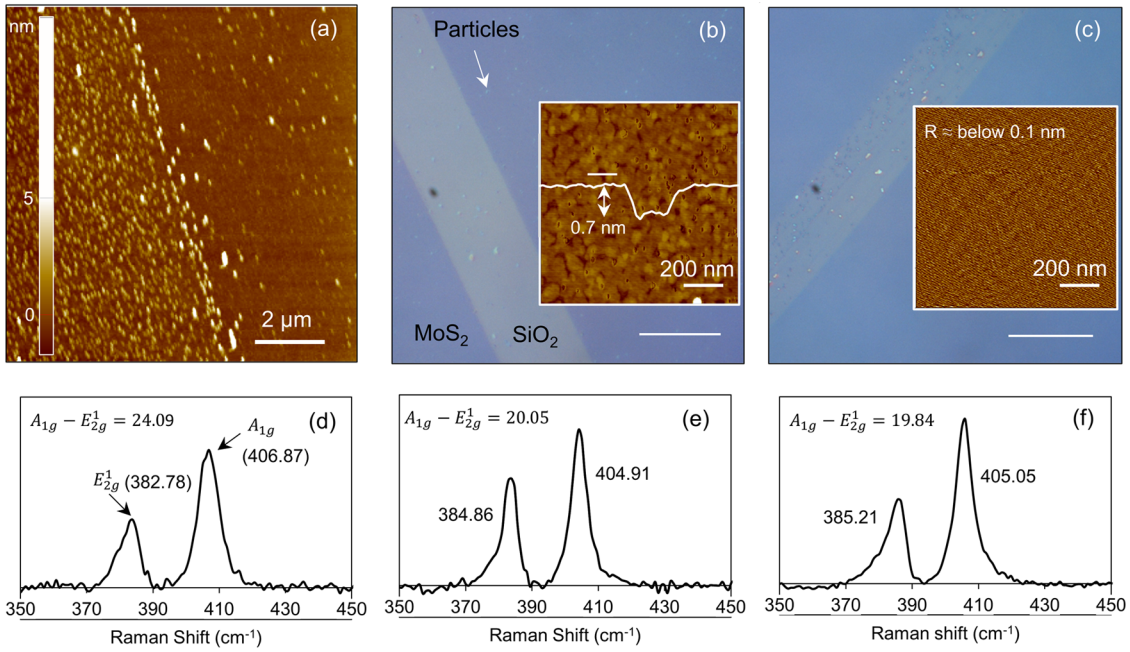

Figure 2. (a) 10 μm × 10 μm AFM scan of the deposited MoS_2 with the $F_{16}CuPc$-excluded solution. Optical microscopic images and 1 μm × 1 μm AFM (inset) images of the deposited MoS_2 with (b) only Na-excluded, the size of AFM line scan is 150 nm, and of (c) both $F_{16}CuPc$- and Na-included solutions, respectively. The scale bar of the optical microscopy images is 20 μm. (d–f) Raman spectra of the relevant MoS_2; for all graphs, the *y*-axis is the intensity (arbitrary unit). All of the data are taken 0.5 mm away from the coating. Here, the noncontact mode along with a 2 nm (tip size) high-profile tip is used for all of the AFM scans.

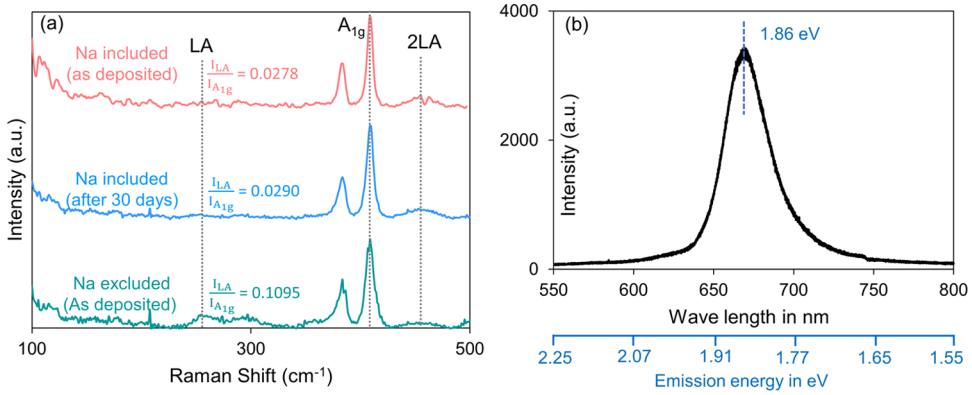

Figure 3. (a) Raman spectra of Na-included (Figure 2c representative sample) and Na-excluded (Figure 2b representative sample) samples, taken 0.5 mm away from the coating. The spectra have been normalized to the intensity of the A_{1g} peak. (b) Photoluminescent spectra of the synthesized MoS_2 (Figure 2c representative sample).

0.0278 for the as-deposited sample and 0.0290 for the sample after 30 days). Therefore, the synthesized MoS_2 was confirmed to have good stability under atmospheric conditions.

Further, a photoluminescent spectrum was taken for the optimized MoS_2 film (the representative sample in Figure 2c). According to Figure 3b, the band gap of the synthesized MoS_2 was calculated, and it showed a band energy of 1.86 eV.

To elucidate the crystal growth, MoS_2 was synthesized at a lower temperature (700 °C), in which individual MoS_2 crystals could be seen by AFM scanning. Figure 4 shows the synthesized MoS_2 using all Mo-, Na-, and $F_{16}CuPc$-containing solutions. Raman spectra and AFM images were taken at different distances from the coated area, as shown in the inset of Figure 4a. According to the Raman spectra shown in Figure 4a, the synthesized MoS_2 showed A_{1g}–E^1_{2g} of 19.99–20.42 cm^{-1} at 0.5 mm—at 4 mm away from the coating (refer to Figure S4 of the SI for the individual spectrum). Over the 4 mm distance, the Raman signals were insignificant. According to Figure 4b–d, MoS_2 monolayer crystals appeared between the distances of 0.5 and 3.5 mm, and they showed a layer thickness of approximately 0.6 nm. Therefore, the Raman spectra and AFM scans confirmed the monolayer structure of the synthesized MoS_2.

However, just outside the solution-coated area (within the first 50 μm), the Raman spectra showed A_{1g}–E^1_{2g} at 25.19 cm^{-1}; Figure S5 of the SI shows the relevant AFM image and line scan. The MoS_2 domains appear as triangular-shaped multilayers, which may be attributable to the high mass flux rate near the coating.

Table 1 lists the physical parameters of the MoS_2 domains represented in Figure 4c–e. The parameters were calculated through image processing using ImageJ software. The surface coverage was highest near the source, which was nearly 70% at a distance of 0.5 mm. In addition, the area coverage gradually

https://doi.org/10.1021/acsomega.1c05052
ACS Omega 2021, 6, 32208–32214

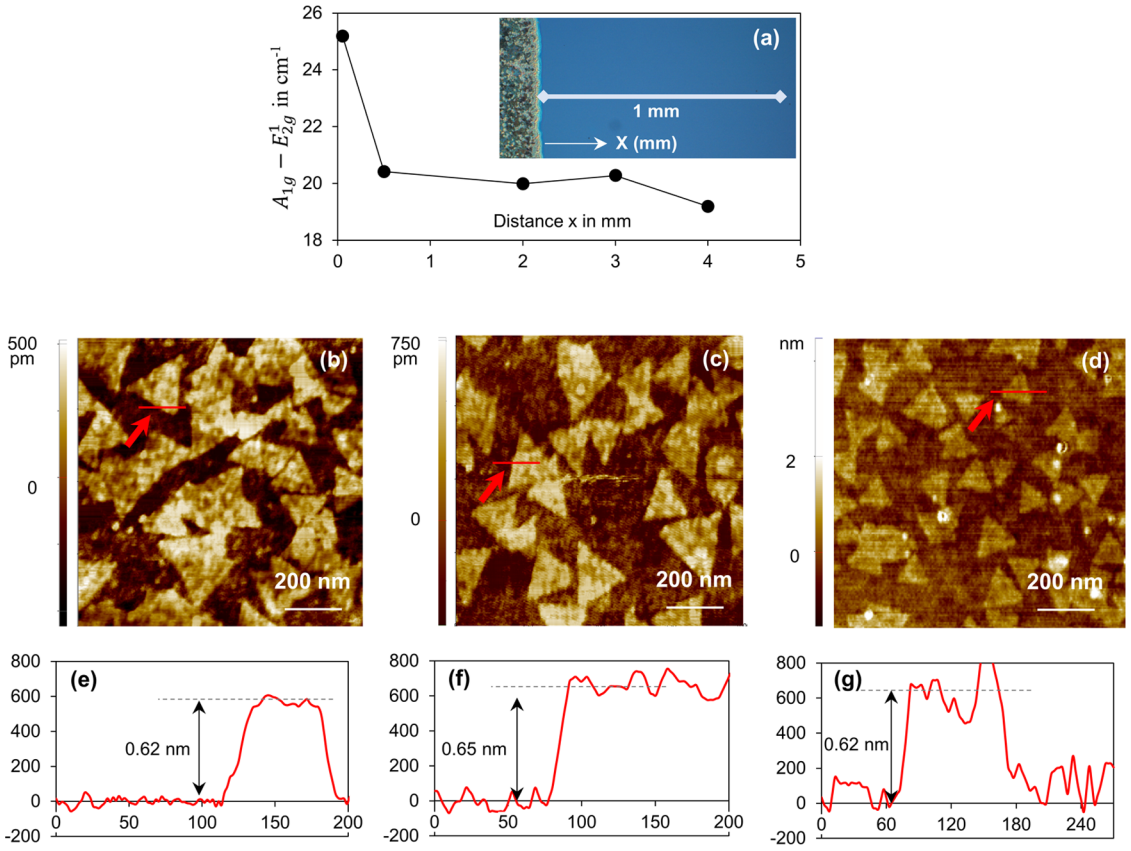

Figure 4. (a) $A_{1g}-E^1_{2g}$ depending on the distance *x*, and the inset is an optical microscopy image of the real sample. AFM images of the synthesized MoS_2 depending on the distance among (b) 0.5 mm, (c) 2 mm, and (d) 3.5 mm; the scanned area of all of the images is 1 μm × 1 μm. (e−g) the line scans of representative AFM figures; in all of the graphs, the *x*-axis is the scan distance in nm, while the *y*-axis is the *z*-scan in pm. Here, the contact mode was used for all AFM scans with 4 nN force.

Table 1. Physical Parameters of the MoS_2 Grains Depending on Location

sample (distance from the coating, mm)	0.5	2	3.5
area coverage (%)	69.49	39.85	36.63
average domain size (nm^2)	1708	1530	893
domain density (number of domains per 1 μm^2)	36	26	41

decreases with distance. Surface coverage depends on the supply of Mo and S, which are highest near the source due to high mass flux.[10] The domain size and density also depended on the distance from the source, as the lowest domain density appeared at the 2 mm distance while the highest density was observed at the longest distance (3.5 mm).

The domain size was calculated by dividing the surface coverage by the number of domains. The largest domain size (1708 nm^2) was observed at a low distance of 0.5 mm. The domain sizes of TMDs are dependent on the combined effects of nuclei density, mass flux, and domain growth rate.[10] In general, higher concentrations of the seeding promoter result in higher nuclei density, which facilitates the smaller domain size due to the growth of multiple domains, instead of a single domain, under limited mass flux.[10] According to diffusion theory, the highest mass flux concentration is available near the

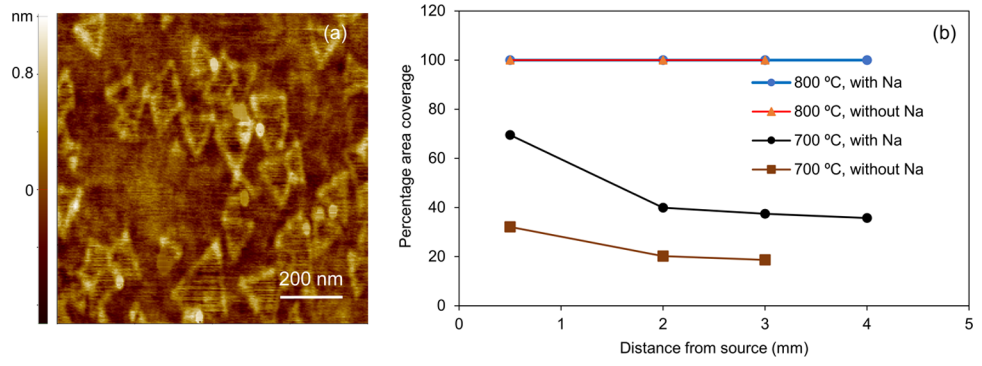

Figure 5. (a) Noncontact mode AFM image of MoS_2, which is synthesized at 700 °C without Na, 1 μm × 1 μm scan. (b) Percentage of area coverage of MoS_2 with various distances from the source.

https://doi.org/10.1021/acsomega.1c05052
ACS Omega 2021, 6, 32208−32214

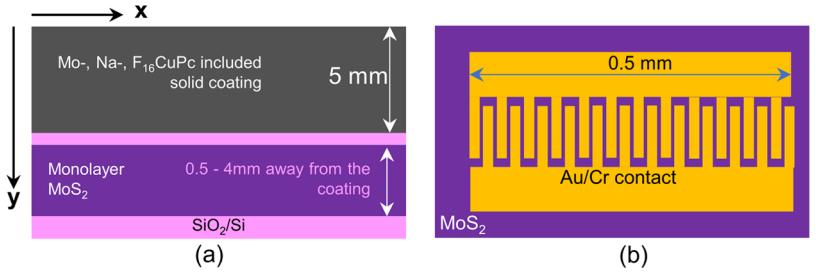

Figure 6. Schematic diagram of the (a) usable region of MoS_2 for device applications and (b) design of a possible photodetector from the current technique (figures are not to scale).

source, so the highest seeding promoter should be concentrated near the source; this is confirmed by the highest nuclei density being at 0.5 mm, compared to that at a 2 mm distance. In spite of the higher nuclei density near the source, the higher Mo and Na flux rates facilitate the increased growth of domains due to the excess materials and the lowered edge-attachment barrier, which is consistent with the previous results.[12,13]

However, the distance far away from the coated area (3.5 mm away) shows a much higher domain density. Further, the 4 mm distance was associated with the smallest domain size and the highest domain density; refer to Figure S6 of the SI for the relevant data. According to Ling et al., a higher concentration of seeding promoters increases the number of domains.[14] However, according to Lin et al., over longer distances, the domain density can be increased due to insufficient source supply.[20] The same reason may apply here, too; the insufficient resources decrease the average crystal size, and the limited resources assist in forming individual grains rather than contributing to the growth of a larger crystal.

Figure 5a shows the synthesized MoS_2 at 700 °C with the Na-excluded solution; the image was taken 500 μm away from the source. Here, the area coverage was 32.06%, the domain density was 35 domains/μm^2, and the average domain size was 916 nm^2. It can clearly be seen that both the Na-excluded and -included samples have a similar domain density, while Na-excluded samples have a much smaller domain size and reduced area coverage. The concentrations of Mo and $F_{16}CuPc$ were similar in both samples; therefore, the existence of Na showed a strong influence on the MoS_2 growth, which is highlighted not only at 700 °C but also at 800 °C, where MoS_2 showed nano-size voids, as discussed previously.

Figure 5b illustrates the variations in percentage of area coverage with the distance from the source under different conditions. At 800 °C, both Na-included and -excluded samples showed full surface coverage, except for the nanoscale voids in the Na-excluded sample, as discussed earlier. However, at 700 °C, the effect of Na was significant, as the Na-included sample had almost twice the area coverage of the Na-excluded sample depending on each position. Thus, in addition to the formation of a void-free film through alkali ion-assisted growth, these results confirm that the alkali ion had the effect of improving area coverage at a relatively lower temperature.

Importance of the Current Technique and Device Design. The proposed technique only requires all-ingredient-based ink, meaning that the amount of the seeding promoter and solid precursor can be adequately controlled. Most importantly, the coating can be applied in a well-selected position within a substrate with a wide range of precise amounts of material quantities. Further, the Mo ion, Na ion, and seeding promoter diffusion distance remain consistent, which is attributed to MoS_2 growing next to the coating. During the diffusion process, the exposed surface area is important for maintaining a consistent mass flux rate. Compared to those in a powder precursor, the true and projected surface areas in a coating-based solid precursor are approximately similar. Therefore, the current technology can provide a consistent and controllable surface area for diffusion-based TMD growth. The consistency in diffusion distance, precise controllability of the ingredient amount, and applicability of a wide range of material quantities makes this technique unique and highly repeatable compared to the conventional CVD technique.

Figure 6a shows the usable region of MoS_2 that is synthesized in the present work. The length is not limited to the *x*-direction, but the device design should be carefully selected in the *y*-direction because it is limited to a length of 3−3.5 mm. Therefore, devices should be limited to the millimeter scale, which is acceptable for most applications because 2D semiconductor-based components such as photodetectors and transistors are designed in a range from nanometer to micrometer scale. The 2D TMDs are primarily used in electronics and optoelectronics such as transistors, photodetectors, and solar cells. The current technique is expected to find potential use in photodetectors, and Figure 6b shows a schematic diagram of a possible design.

CONCLUSIONS

MoS_2 was synthesized using a controlled amount of Mo with localized diffusion. The Raman characteristics and AFM imagery indicate that the presence of Na is essential for achieving a void-free continuous film using this technique. Due to the rapid mass flux and lowered edge-attachment barrier, the effectiveness of the process was dependent on the processing temperature and the presence of. At 800 °C, a void-free continuous film of MoS_2 was observed, while at 700 °C, triangular-shaped domains appeared. Both the area coverage and domain size gradually decreased at positions further away from the source. At 800 °C, the Na-free condition fails to provide a void-free film, and at 700 °C, it shows an area coverage and a domain size that are much lower in comparison. Further, this proposed technique makes it easy to fabricate a millimeter-scale void-free MoS_2 film with a 1.86 eV band gap.

MATERIALS AND METHODS

To begin, 0.5 mL of 0.1 M MoO_3 (99.995%) and 0.5 M (NaCl) in NH_4OH solution were mixed with 0.5 mL of $F_{16}CuPc$ solution (1 mg of $F_{16}CuPc$ dissolved in 100 mL of

https://doi.org/10.1021/acsomega.1c05052
ACS Omega 2021, 6, 32208−32214

NH_4OH); the resulting solution was further diluted with another 1.5 mL of NH_4OH prior to its application on the SiO_2 (280 μm)/Si substrate. At this point, 2 μL of the solution was spread on a 0.5 cm^2 area (the other half of the substrate was kept uncontaminated) of the piranha-treated substrate (to improve wettability), followed by 10 min of oven drying at 60 °C. The solution was coated by scanning the micropipette tip. The sample was then placed with the uncoated area facing downstream. An excess amount of S of 50−60 mg was kept in the upstream of the CVD chamber (low-temperature zone), whereas the main zone just reached the processing temperature at which S began to melt. CVD was raised to process temperature under vacuum (below 1 mTorr), followed by MoS_2 growth under a N_2 (99.99%) atmosphere at 300−400 mTorr pressure for 5 min. Finally, samples were cooled within the chamber under vacuum. The analyses used for characterization were Raman spectroscopy, atomic force microscopy (AFM), photoluminescent spectroscopy (PL), and optical microscopy (OM).

■ ASSOCIATED CONTENT

Supporting Information

The Supporting Information is available free of charge at https://pubs.acs.org/doi/10.1021/acsomega.1c05052.

UV−vis spectra of F_{16}CUPc solution, including photographs of relevant solutions; EDX spectra of the ink-coated substrate, including EDX maps of all of the components and MoS_2 film (point scan); optical microscopy images of the synthesized MoS_2 film; all of the Raman spectra of MoS_2 depending on the distance from the ink-coated area; and AFM images, including line scan and crystal size analysis (PDF)

■ AUTHOR INFORMATION

Corresponding Authors

Sung Woon Cho − *Department of Advanced Components and Materials Engineering, Sunchon National University, Suncheon, Jeonnam 57922, South Korea;* orcid.org/0000-0001-8392-3668; Email: swcho@scnu.ac.kr

Ji-Myon Lee − *Department of Advanced Components and Materials Engineering, Sunchon National University, Suncheon, Jeonnam 57922, South Korea;* orcid.org/0000-0002-5389-041X; Email: jimlee@scnu.ac.kr

Authors

Maddumage Don Sandeepa Lakshad Wimalananda − *Department of Advanced Components and Materials Engineering, Sunchon National University, Suncheon, Jeonnam 57922, South Korea*

Jae-Kwan Kim − *Department of Advanced Components and Materials Engineering, Sunchon National University, Suncheon, Jeonnam 57922, South Korea*

Complete contact information is available at: https://pubs.acs.org/10.1021/acsomega.1c05052

Author Contributions

The manuscript was written through the contributions of all authors. All authors have given approval to the final version of the manuscript.

Notes

The authors declare no competing financial interest.

■ ACKNOWLEDGMENTS

This research was supported by the Basic Science Research Program of the National Research Foundation of Korea (NRF) and funded by the Ministry of Education (NRF-2014R1A6A1030419 and NRF-2021R1I1A1A01051227).

■ ABBREVIATIONS

TMD, transition metal dichalcogenides; CVD, chemical vapor deposition; PTAS, perylene 3,4,9,10-tetracarboxylic potassium salt; F_{16}CuPc, copper(II) 1,2,3,4,8,9,10,11,15,16,17,18,22,23,24,25-hexadecafluoro-29*H*,31*H*-phthalocyanine; AFM, atomic force microscopy; PL, photoluminescent spectroscopy

■ REFERENCES

(1) Yazyev, O. V.; Louie, S. G. Electronic Transport in Polycrystalline Graphene. *Nat. Mater.* **2010**, *9*, 806−809.

(2) Zhang, Y.; Tang, T. T.; Girit, C.; Hao, Z.; Martin, M. C.; Zettl, A.; Crommie, M. F.; Shen, Y. R.; Wang, F. Direct Observation of a Widely Tunable Bandgap in Bilayer Graphene. *Nature* **2009**, *459*, 820−823.

(3) Li, X.; Zhu, H. Two-Dimensional MoS 2: Properties, Preparation, and Applications. *J. Materiomics* **2015**, *1*, 33−44.

(4) Krishnan, U.; Kaur, M.; Singh, K.; Kumar, M.; Kumar, A. A Synoptic Review of MoS 2: Synthesis to Applications. *Superlattices Microstruct.* **2019**, *128*, 274−297.

(5) Velický, M.; Toth, P. S. From Two-Dimensional Materials to Their Heterostructures: An Electrochemist's Perspective. *Appl. Mater. Today* **2017**, *8*, 68−103.

(6) Hong, S.; Sheng, C.; Krishnamoorthy, A.; Rajak, P.; Tiwari, S.; Nomura, K. I.; Misawa, M.; Shimojo, F.; Kalia, R. K.; Nakano, A.; Vashishta, P. Chemical Vapor Deposition Synthesis of MoS 2 Layers from the Direct Sulfidation of MoO 3 Surfaces Using Reactive Molecular Dynamics Simulations. *J. Phys. Chem. C* **2018**, *122*, 7494−7503.

(7) Wen, Y. Y.; Zeng, X. B.; Chen, X. X.; Wang, W. Z.; Ding, J.; Xu, S. E. *Synthesis of Monolayer MoS2 by CVD Approach*, Proceedings of the 2nd Annual International Conference on Advanced Material Engineering (AME 2016); Atlantis Press, 2016; pp 1034−1039.

(8) Chen, J.; Tang, W.; Tian, B.; Liu, B.; Zhao, X.; Liu, Y.; Ren, T.; Liu, W.; Geng, D.; Jeong, H. Y.; Shin, H. S.; Zhou, W.; Loh, K. P. Chemical Vapor Deposition of High-Quality Large-Sized MoS 2 Crystals on Silicon Dioxide Substrates. *Adv. Sci.* **2016**, *3*, No. 1500033.

(9) Zhao, Y.; Lee, H.; Choi, W.; Fei, W.; Lee, C. J. Large-Area Synthesis of Monolayer MoSe2 Films on SiO2/Si Substrates by Atmospheric Pressure Chemical Vapor Deposition. *RSC Adv.* **2017**, *7*, 27969−27973.

(10) You, J.; Hossain, M. D.; Luo, Z. Synthesis of 2D Transition Metal Dichalcogenides by Chemical Vapor Deposition with Controlled Layer Number and Morphology. *Nano Convergence* **2018**, *5*, No. 26.

(11) Jo, S.; Jung, J. W.; Baik, J.; Kang, J. W.; Park, I. K.; Bae, T. S.; Chung, H. S.; Cho, C. H. Surface-Diffusion-Limited Growth of Atomically Thin WS 2 Crystals from Core-Shell Nuclei. *Nanoscale* **2019**, *11*, 8706−8714.

(12) Ju, M.; Liang, X.; Liu, J.; Zhou, L.; Liu, Z.; Mendes, R. G.; Rümmeli, M. H.; Fu, L. Universal Substrate-Trapping Strategy to Grow Strictly Monolayer Transition Metal Dichalcogenides Crystals. *Chem. Mater.* **2017**, *29*, 6095−6103.

(13) Lu, Y.; Chen, T.; Ryu, G. H.; Huang, H.; Sheng, Y.; Chang, R.-J.; Warner, J. H. Self-Limiting Growth of High-Quality 2D Monolayer MoS 2 by Direct Sulfurization Using Precursor-Soluble Substrates for Advanced Field-Effect Transistors and Photodetectors. *ACS Appl. Nano Mater.* **2019**, *2*, 369−378.

(14) Ling, X.; Lee, Y. H.; Lin, Y.; Fang, W.; Yu, L.; Dresselhaus, M. S.; Kong, J. Role of the Seeding Promoter in MoS2 Growth by Chemical Vapor Deposition. *Nano Lett.* **2014**, *14*, 464−472.
(15) Gao, Q.; Zhang, Z.; Xu, X.; Song, J.; Li, X.; Wu, Y. Scalable High Performance Radio Frequency Electronics Based on Large Domain Bilayer MoS 2. *Nat. Commun.* **2018**, *9*, No. 4778.
(16) Gnanasekar, P.; Periyanagounder, D.; Nallathambi, A.; Subramani, S.; Palanisamy, M.; Kulandaivel, J. Promoter-Free Synthesis of Monolayer MoS2 by Chemical Vapour Deposition. *CrystEngComm* **2018**, *20*, 4249−4257.
(17) Liu, K. K.; Zhang, W.; Lee, Y. H.; Lin, Y. C.; Chang, M. T.; Su, C. Y.; Chang, C. S.; Li, H.; Shi, Y.; Zhang, H.; Lai, C. S.; Li, L. J. Growth of Large-Area and Highly Crystalline MoS 2 Thin Layers on Insulating Substrates. *Nano Lett.* **2012**, *12*, 1538−1544.
(18) Li, H.; Zhang, Q.; Yap, C. C. R.; Tay, B. K.; Edwin, T. H. T.; Olivier, A.; Baillargeat, D. From Bulk to Monolayer MoS 2: Evolution of Raman Scattering. *Adv. Funct. Mater.* **2012**, *22*, 1385−1390.
(19) Mignuzzi, S.; Pollard, A. J.; Bonini, N.; Brennan, B.; Gilmore, I. S.; Pimenta, M. A.; Richards, D.; Roy, D. Effect of Disorder on Raman Scattering of Single-Layer Mo S2. *Phys. Rev. B* **2015**, *91*, No. 195411.
(20) Lin, Z.; Zhao, Y.; Zhou, C.; Zhong, R.; Wang, X.; Tsang, Y. H.; Chai, Y. Controllable Growth of Large-Size Crystalline MoS2 and Resist-Free Transfer Assisted with a Cu Thin Film. *Sci. Rep.* **2016**, *5*, No. 18596.

https://doi.org/10.1021/acsomega.1c05052
ACS Omega 2021, 6, 32208−32214